Energy and Buildings 64 (2013) 162–171

Contents lists available at SciVerse ScienceDirect

Energy and Buildings

journal homepage: www.elsevier.com/locate/enbuild

Energy simulation of sustainable air-cooled chiller system for commercial buildings under climate change

F.W. Yu [a,*], K.T. Chan [b], Rachel K.Y. Sit [a,b], J. Yang [b]

[a] Hong Kong Community College, The Hong Kong Polytechnic University, Hong Kong, China
[b] Department of Building Services Engineering, The Hong Kong Polytechnic University, Hong Kong, China

ARTICLE INFO

Article history:
Received 12 November 2012
Received in revised form 10 January 2013
Accepted 30 April 2013

Keywords:
Air-cooled chiller
Optimal condenser fan speed control
Mist pre-cooling
Simulation

ABSTRACT

Air-cooled chiller systems are commonly used to provide cooling energy in commercial buildings but with considerable electricity consumption. This study demonstrates how to operate the systems with sustainable performance under climate change by applying optimal condenser fan speed control coupled with mist pre-cooling of air entering the condensers. The simulation of system performance was carried out by using EnergyPlus together with an experimentally verified chiller model capable of analyzing advanced control strategies. Weather data under three climate change scenarios in 2020, 2050 and 2080 were considered in evaluating the cooling demand and hourly electricity consumption of an air-cooled chiller system serving an office building. It is found that optimal condenser fan speed control coupled with mist pre-cooling of air-cooled condensers can help maintain a higher coefficient of performance under the warmer future climate, reducing the annual electricity consumption by 16.96–18.58% in the reference weather year and 2080. The ways to implement the sustainable control have been discussed.

1. Introduction

Chiller systems are commonly used to provide cooling energy in the form of chilled water in commercial buildings in subtropical or hot and arid zones. The operation of chiller systems can account for the highest proportion of the total electricity used in commercial buildings [1]. The energy performance of chillers depends greatly on the heat rejection systems used. Where water conservation is concerned, using air-cooled chillers is unavoidable, though their energy performance is lower than chillers using water-cooled heat rejection systems [2]. The energy performance of air-cooled chillers is described by the coefficient of performance (COP)—the cooling capacity output in kW divided by the electric power input in kW. The variation of COP depends on the temperature of air entering the condenser and the way to control the condensing temperature. Most existing air-cooled chillers operate under head pressure control (HPC) under which the condensing temperature is kept at 15–20 °C above the dry bulb temperature of outdoor air in all loading conditions. This disregards an optimal trade-off between the compressor power and condenser fan power to maximize the COP at part load operation. The HPC leads to the inferior performance of air-cooled chillers compared with water-cooled chillers operating with a lower condensing temperature in the range of 30–40 °C. Depending on capacity, the nominal COP of air-cooled chillers is 2.6–2.9 at full load with the temperature of air entering the condenser at 35 °C [2], while a few modern highly efficient products using variable speed compressors are claimed to have a nominal COP of 3.2 with superior COP at part load operation. In fact, there is no rapid improvement in the COP of air-cooled chillers as the advancements are limited to the use of variable speed control to the compressors and condenser fans, and to the enhanced heat exchange performance of the evaporators and condensers. HPC remains to be used even for highly efficient products.

Some studies have discussed essential design principles and operating strategies to improve the performance of chiller systems. Chan et al. [3] addressed the need to perform accurate and detailed calculation of a cooling load profile in order to avoid unnecessary spare system capacity while ensuring system reliability. Techniques to optimize the COP of air-cooled chillers are: floating condensing temperature control (CTC); variable primary flow to chiller evaporators; risk-based preventative maintenance through a sophisticated chiller plant control system. Chang [4] and Lee et al. [5] applied an evolution strategy (an optimization tool) to solve the optimum loading problem of multiple chillers. To allow chillers to operate at different part load ratios, each chiller should be coupled with a variable speed chilled water pump. However, variable flow control is seldom applied to chillers in most existing chiller systems. This is due to the higher initial cost of variable speed drives and a concern over the safe operation of chillers at off-design chilled water flow rates. Sun et al. [6] proposed a fused measurement of

* Corresponding author. Tel.: +852 37460416; fax: +852 23647375.
E-mail address: ccyufw@hkcc-polyu.edu.hk (F.W. Yu).

0378-7788/$ – see front matter © 2013 Elsevier B.V. All rights reserved.
http://dx.doi.org/10.1016/j.enbuild.2013.04.027

Nomenclature

a_0 to a_5	regression coefficients for CAPFT
b_0 to b_5	regression coefficients for EIRFT
c_0 to c_5	regression coefficients for EIRFPLR
CAPFT	regression function for chiller capacity
COP	coefficient of performance
CTC	floating condensing temperature control
C_{pa}	specific heat capacity of air (assumed to be 1.02 kJ/kg °C)
C_{pw}	specific heat capacity of water (assumed to be 4.19 kJ/kg °C)
E	power input (kW)
EIRFT	regression function for compressor efficiency
EIRFPLR	regression function for compressor efficiency at part load conditions
Eff_{cd}	condenser heat transfer effectiveness
h_{db}	specific enthalpy with dry bulb temperature (kJ/kg)
HPC	head pressure control
m	mass flow rate (kg/s)
OCFSC	optimal condenser fan speed control
PLR	chiller part load ratio
R	rotating speed (% of full speed)
RH	relative humidity (%)
Q_{cd}	heat rejection (kW)
Q_{cl}	chiller load (kW)
T	temperature (°C)
V_a	airflow provided by the operating condenser fans (m^3/s)
W	moisture content (kg/kg of dry air)
ρ_a	air density (assumed to be 1.2 kg/m^3)
η_{dc}	cooling effectiveness of direct evaporative cooler
ΔW	change in moisture content of outdoor air (kg/kg of dry air)

Subscripts

cc	compressor
ch	chiller
cd	condenser or at the condenser side
cdae	air entering the condenser
cdal	air leaving the condenser
chwr	chilled water returned to the chiller
chws	chilled water supplied by the chiller
cf	condenser fan
db	dry bulb
db′	dry bulb with mist pre-cooling
ev	evaporator or at the evaporator side
mist	mist generation
w	chilled water
wb	wet bulb
rated	at rated conditions

building cooling loads and indirect indicators of cooling loads to enhance the reliability of chiller sequencing control with improved energy efficiency. Yet the fused measurement relies on a comprehensive monitoring of operating data related to the cooling load calculation and other operating data associated with the power of chillers and pumps. Some existing chiller systems appear to operate with sub-standard monitoring devices with incomplete data logging facilities. This affects the implementation of optimal chiller sequencing control. Through detailed energy audits on chiller systems serving an industrial building and an institutional building, Song et al. [7] and Saidur et al. [8] addressed the energy saving benefits of applying variable speed drives to chillers, chilled water pumps, condenser water pumps and cooling tower fans. Yet the all-variable speed design is not increasingly applied to new chiller systems. It is admitted that system operators may hesitate to manage the variable speed system components relying on sophisticated automatic control.

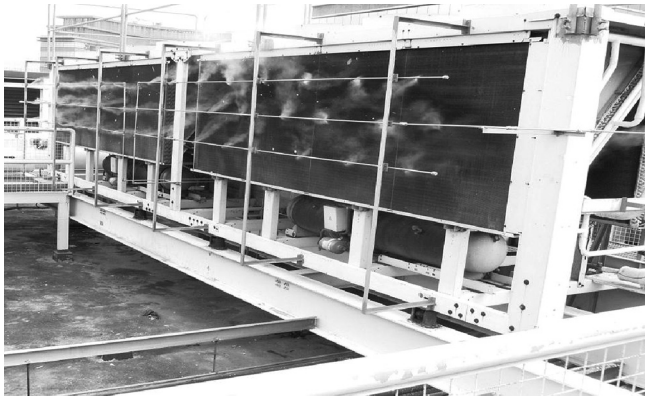

Fig. 1. Pipe and nozzle layouts of a mist system for the condenser of an existing air-cooled chiller.

Contrary to HPC, CTC has been identified to be an effective means to improve the COP of air-cooled chillers at part load operation [9,10]. Yet CTC is not developed as a standard feature for modern air-cooled chiller products. The condenser fans under CTC run at optimal number and speed to minimize the sum of compressor power and condenser fan power for all operating conditions. Given that the rated fan power generally accounts for less than 10% of the rated compressor power in typical condenser design, the total power can be minimized by allowing the condensing temperature to be slightly above the dry bulb temperature of outdoor air under light load conditions. Following this principle, it is possible to further increase their COP by lowering the temperature of air entering the condenser.

Evaporative cooling is a common means to reduce the temperature of outdoor air from its dry bulb to wet bulb [11–15] via a constant enthalpy process. To provide the evaporative cooling effect, Zhang et al. [12] made use of a pack of corrugated holed aluminum foils to trap a water film in front of an air-cooled condenser. Such a cooler allows the dry bulb temperature of the air stream to approach its wet bulb temperature following an adiabatic cooling process but with an increased fan power due to the additional airflow resistance by the cooler. The experimental study showed that the cooling effectiveness of the cooler (η_{dc}) was identified to be about 0.8. η_{dc} is defined as $(t_1 - t_2)/(t_1 - t_w)$, where t_1 and t_2 are temperatures of air at the inlet and outlet of the cooler, respectively, and t_w is the wet bulb temperature of air at the inlet—the theoretical lowest t_2. A η_{dc} of below one suggests that t_2 can never approach the corresponding t_w. Given a η_{dc} of 0.8, it is still possible to reduce the dry bulb temperature by 3–10 °C under a warm-humid climate. Hajidavalloo and Eghtedari [13] carried out another experimental test on the performance of an evaporative cooler with a cellulous media pad installed in front of the condenser of a room air-conditioner. The results indicated that the cooler brought a 6.1–13.3% increase in the refrigeration effect and a 31.7–50.6% rise in the COP over the ambient dry bulb temperatures ranging between 35 °C and 49 °C. The improvement in the COP is more significant at higher ambient temperatures.

Alternatively, evaporative cooling can be achieved by spraying mist directly in front of an air-cooled condenser [14,15]. As Fig. 1 illustrates, a mist pre-cooling system can be installed easily for an existing chiller at no modification. The cooling effectiveness will approach to one if a sufficient amount of mist droplets are fully vaporized on the condenser coil. Such a mist pre-cooling system

does not cause any flow resistance to the air stream and therefore no additional fan power will be incurred. The electric power required to drive the high pressure pump is about 23 kW per unit of mist generation rate in kg/s. The mist generation rate required is around 0.0002 kg/s per unit of cooling capacity in kW. Regarding cooling towers designed with a condenser water flow rate of 0.053 kg/s per unit of cooling capacity in kW [16], the water make up rate is 0.0016 kg/s per unit of cooling capacity in kW (i.e. 3% of condenser water flow rate). Given this, the water consumption rate of mist pre-cooling for air-cooled chillers accounts for only 12.5% of that for water-cooled chillers. Where water conservation is concerned, using air-cooled chillers is more preferable than water-cooled chillers. It is therefore worth exploiting mist pre-cooling in a retrofit application for existing installations and in an integrated design with new installations, in order to enhance the low energy feature of air-cooled chillers.

Lam et al. [17] illustrated that the electricity consumption of a chiller plant varies with climatic variables. The future warmer climate can cause a severe rise in energy use by the building sector if the COP of chiller systems has no improvement. While variable speed drives facilitate the COP improvement of water-cooled chillers, there is no significant increase in the COP of modern air-cooled chillers as constrained by HPC and the conventional design of multiple condenser fans at fixed speed. It is an under research area on how mist pre-cooling of air-cooled condensers coupled with optimal condenser fan speed control helps alleviate the energy impacts of air-cooled chiller systems under climate change. The potential benefits of mist pre-cooling of condenser air have been identified in some existing air-cooled chillers under HPC [14,15,18]. Yet the fixed condensing temperature setting in the existing chillers place a constraint on exploring further improvement in the COP when mist pre-cooling is integrated with optimal condenser fan control. To promote mist pre-cooling to be a standard feature for improving the COP of air-cooled chillers in new design in a long run, the effectiveness of a mist system under climate change scenarios should be addressed. Different from previous research work by authors on mist-precooling for air-cooled chillers [14,15,18–20], this study further explores the potential benefits of air-cooled chillers integrated with a mist pre-cooling system throughout their operating life under climate change. A parametric study in terms of correlation analysis will be carried out to examine how to achieve an optimal mist generation rate in response to the condenser fan speed control under various combinations of chiller load and weather conditions.

Drawing on previous experimental and simulation studies on air-cooled chiller systems, this study aims at providing a detailed analysis on how the advanced control enables air-cooled chillers to operate with sustainable performance throughout their working life under climate change. First, the generation of climate change scenarios will be described. The typical arrangement of a mist system with air-cooled condensers will be explained. Simulation procedures will then be given on how EnergyPlus was used to model an air-cooled chiller system serving a reference office building and to identify the electricity consumption of chillers operating with conventional and advanced controls. Discussions will be made on how to optimize the control of mist pre-cooling for air-cooled chillers operating under the HPC and the optimal condenser fan speed control. The significance of this study is to demonstrate how to enhance the sustainability of air-cooled chiller systems under climate change.

2. Generation of climate change scenarios

A typical meteorological year (TMY) weather file is often required for hour-by-hour building energy simulation. Chan et al. [21] developed a TMY weather file for Hong Kong which is in the epw format for use in EnergyPlus [22]. The TMY file forms the present-day file representing typical weather data over a 25-year period from 1979 to 2003. It contains composite sets of hourly weather data from multiple years in the monitoring period. Each month comprising the TMY was selected to represent prevailing weather conditions of the same month over the entire period. Table 1 shows some key variables and their ranges for Hong Kong.

Given a TMY weather file, it is possible to generate future weather data under climate change. According to Guan's review [23], approaches to generating future weather data were classified as the extrapolating statistical method, the stochastic weather model, the imposed offset method and the global climate model. The statistical method is limited to forecast degree-day data by extrapolating historical data, which is not applicable for generating hourly data in the TMY format. The stochastic weather model draws on only inputs of a few weather variables to generate an artificial meteorological database for many years through a complicated modeling process. Because of the stochastic nature, accuracy is not ensured in modeling many climatic variables and the possible relationship between the climatic variables is discounted. This may fail to consider the link between the various weather variables and certain temperature rise scenarios due to global warming.

In the imposed offset method, hourly weather data are forecasted based on a set of current reference data in the TMY or other similar formats. The algorithms for generating individual weather parameters involve morphing the current data by three operations: (1) shifting; (2) linear stretching (scaling factor); and (3) shifting and stretching. The monthly delta values of the shifting and stretching components can be predicted from General Circulation Models (GCMs) for weather forecasting. A new weather file presenting climate change scenarios is formed with the forecasted hourly dry bulb temperature, humidity ratio, and global, direct normal and diffuse horizontal solar radiation, etc., based on the projected potential temperature increase with different assumptions to link the variation of absolute humidity with the increased temperature. The global climate model draws on historically observed weather data for model calibration and considers the continuous change of atmospheric carbon dioxide concentration which is not readily available from the TMY file. Compared with the imposed offset method, the global climate model is more complicated as it is based on fundamental physical models developed by meteorologists. Considering the simplicity of modeling procedure and the data format requirement for detailed building simulation, the imposed offset method would be the most preferable method to project future weather data modified from current data in a TMY weather file.

The weather generator program CCWorldWeatherGen [24] was used to generate climate change scenarios for Hong Kong in three future periods (2010–2039, 2040–2069 and 2070–2099) represented by three benchmark years of 2020, 2050 and 2080. The program drew on the imposed offset method and was developed based on the Hadley Center Coupled Model, version 3 (HadCM3) under the third assessment report of the Intergovernmental Panel on Climate Change (IPCC) [25]—the leading international body for the assessment of climate change. Among various prediction models based on GCMs, the HadCM3 model is based on about 300 km grid spacing [26] and contains a set of climate change data for four different global carbon emission scenarios: low, medium–low, medium–high and high emissions. These four correspond to the IPCC scenarios B1, B2, A2 and A1F1 which are typically considered to investigate the impact of climate change on energy use in buildings [27]. Lee and Levermore [28] used the HadCM3 model to generate weather data for climate change in order to analyze the trend of building design in South Korea. It is reasonable to draw on some global climate change scenarios like HadCM3 for building energy simulation, in case regional climate change data are not available.

Table 1
Key climatic variables and their ranges in the TMY weather file of Hong Kong.

Month	Year used	Dry bulb temperature (°C)			Global horizontal radiation (MJ/m²)				Wind speed (m/s)	
		Max.	Mean	Min.	Max.	Mean	Min.	Max.	Mean	Min.
January	1995	22.5	16.1	9.3	717	106	0	7.0	2.8	0.5
February	1988	23.3	16.3	10.2	856	112	0	8.0	3.6	0.5
March	2003	26.4	19.0	11.7	881	121	0	8.5	2.9	0.1
April	1986	30.1	22.6	14.8	919	140	0	9.0	3.4	0.0
May	1997	31.3	26.1	21.4	969	153	0	8.0	2.6	0.4
June	1990	32.5	27.9	23.1	936	161	0	11.0	3.3	0.5
July	2000	32.8	28.8	25.0	972	205	0	9.5	3.0	0.4
August	2002	32.7	28.4	24.6	953	180	0	9.0	2.8	0.4
September	1982	32.8	27.5	23.6	933	167	0	9.5	3.7	0.0
October	1984	31.0	25.3	20.6	864	169	0	7.0	3.1	0.0
November	1989	27.8	21.5	12.4	797	144	0	8.0	2.9	0.5
December	1993	24.8	17.1	9.2	725	127	0	8.0	2.9	0.0

The TMY weather file for Hong Kong downloaded at [29] was an input file for the program. The HadCM3 model drew on a morphing procedure to forecast weather data based on data in the present-day file [30]. The assumption involved in the morphing procedure is that the relative humidity will maintain the same for both the current and climate change scenarios. The rationale for the assumption is that the earth temperature under global warming will increase which would lead to more water evaporating to atmosphere to maintain a constant relative humidity. This assumption was supported by Sturman and Tapper [31] and Aguiar et al. [32] if information on future humidity change due to global warming is not available. The IPCC scenario A2 representing medium–high global carbon emissions was used with a rise in the annual average daily mean temperature of 0.74 °C in 2010–2039, 1.69 °C in 2040–2069 and 3.00 °C in 2070–2099.

The hourly data (x) to be morphed include the dry bulb temperature, dew point temperature, global horizontal radiation, direct normal radiation, diffuse horizontal radiation, atmospheric pressure and wind speed. These data influence the cooling load calculation and the operating performance of chiller systems. The algorithm of morphing future hourly data (x) involves shifting and stretching the corresponding present-day data (x_0), as illustrated by Eq. (1), where Δx_m represents the shift part and α_m represents the stretch part for x_0 in the month m. $\langle x_0 \rangle_m$ is the monthly mean of x_0 for month m. Detailed equations for morphing each variable are given in [33].

$$x = x_0 + \Delta x_m + \alpha_m (x_0 - \langle x_0 \rangle_m) \quad (1)$$

Fig. 2 shows simulation results of the key climatic variables (dry bulb temperature and global horizontal radiation) in 2020, 2050 and 2080 in relation to the baseline (TMY). Due to global warming, the dry bulb temperature rises by various degrees from the corresponding baseline. The temperature rise in the later years tends to be higher in winter months than in summer months. One reason for this may be associated with the lower temperatures with greater fluctuation in winter months. In 2020, 2050 and 2080, the monthly mean global horizontal radiation has a different variation pattern in summer and winter months. The decreased radiation in summer months is probably due to a situation where the percentage of cloud cover and the concentration of suspended particulates could increase in the future. The increased radiation in winter months, on the contrary, could be associated with more days with a brighter sky and fewer suspended particulates.

Figs. 3 and 4 show the frequency polygon of the morphed hourly weather data (dry bulb temperature and global horizontal radiation) in January (a typical winter month) and in July (a typical summer month). With a positive Δx_m in Eq. (1), the forecasted hourly dry bulb temperatures increased from their original values in the TMY. This generally results in a rightward shift in the frequency polygon. Regarding the hourly global horizontal radiation, non-sunshine hours were excluded in the plots. The forecasted hourly data have no significant change in January but was morphed irregularly in July, based on the combination of the varying shift component Δx_m and stretch component α_m.

3. Description of mist pre-cooling to air-cooled condensers

Fig. 1 shows an example of pipe and nozzle layouts that produce mist in front of the condenser of an existing air-cooled chiller. As Fig. 5 illustrates, a cloud of very fine water droplets in 10-micron size (mist) are released from low flow atomization nozzles when the pump delivers water along the pipework at a high pressure of around 70 bars. The mist facilitates the evaporative cooling process, allowing the temperature of air entering the condenser to drop from its dry bulb to near wet bulb.

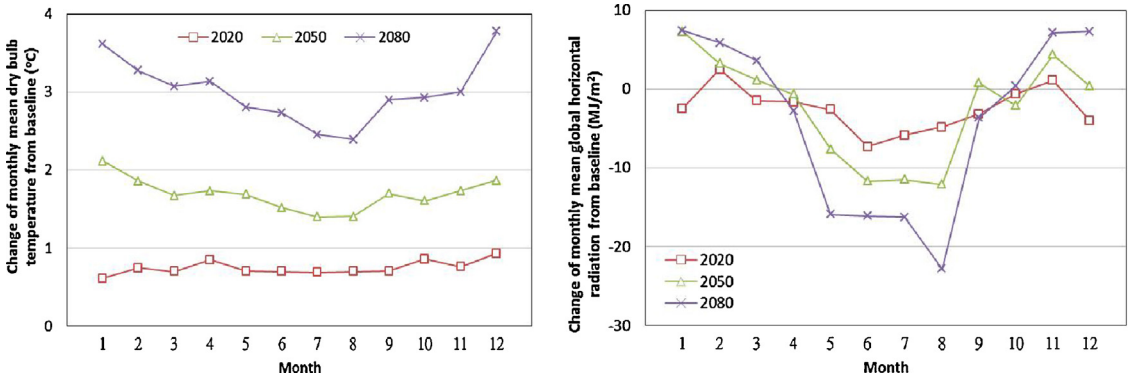

Fig. 2. Change of monthly mean weather data in 2020, 2050 and 2080 from the baseline.

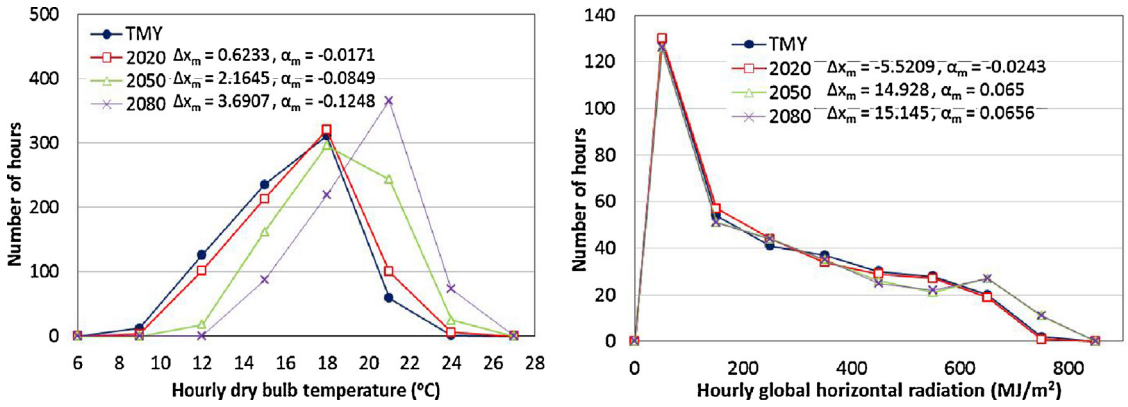

Fig. 3. Frequency distribution of hourly weather data in January in the TMY, 2020, 2050 and 2080.

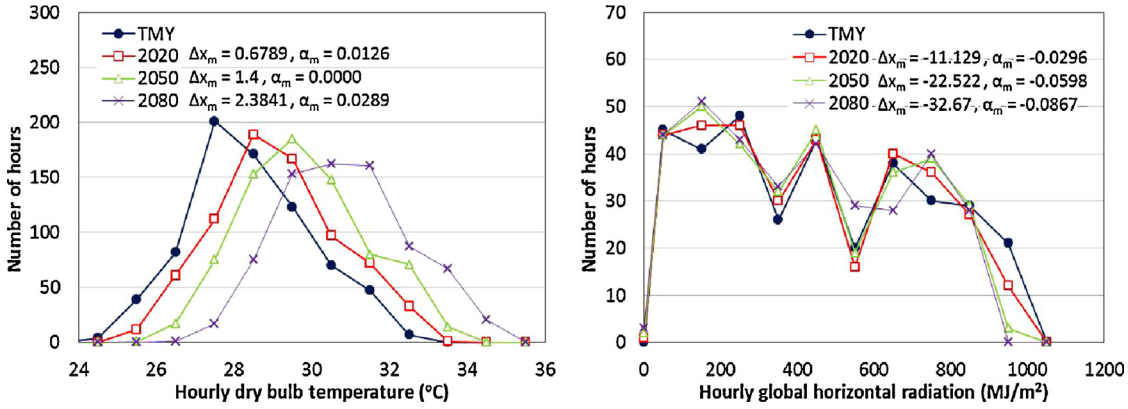

Fig. 4. Frequency distribution of hourly weather data in July in the TMY, 2020, 2050 and 2080.

The design mist generation rate depends on the total heat rejection airflow rate of a chiller and the potential increase in moisture content based on the difference between the dry bulb and wet bulb temperatures. Over-provision of mist causes frequent damping and, in turn, scaling problems on condenser fins and coils while an insufficient amount of mist has no effect on the drop in the dry bulb temperature. Based on each set of hourly weather data in the TMY, the maximum increase in moisture content at 100% relative humidity was identified to be 0.0038 kg/kg of dry air and a moderate level of 0.0018 kg/kg of dry air (at the 80th percentile) was considered to evaluate the design mist generation rate. Given the total heat rejection airflow rate of 140 m^3/s or 168 kg/s for a chiller rated at 1511 kW, the peak mist generation rate was calculated to be $0.0018 \times 168 = 0.30$ kg/s. Following the specifications given by a system supplier, nine sets of high pressure pumps rated at 0.75 kW each with a flow rate of 0.033 kg/s were used for the mist system of each chiller. The mist generation rate could vary from 0.033 to 0.30 kg/s in nine steps in order to match different ambient conditions and heat rejection airflow rates of the chiller. The total pump power accounts for only 19% of the rated condenser fan power.

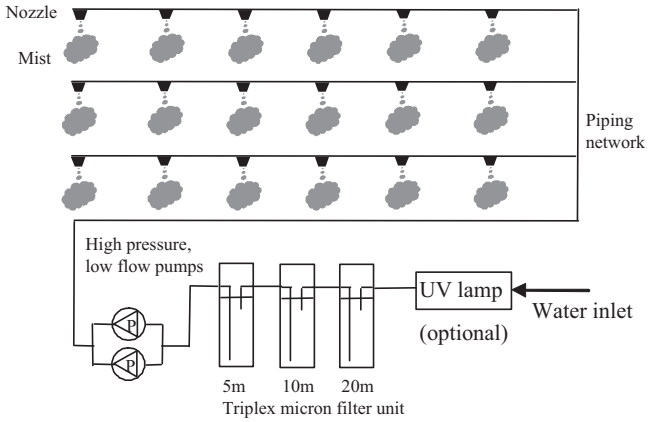

Fig. 5. Schematic diagram of mist system for each chiller.

The proliferation of Legionella by aerosols would be a concern in the evaporative cooling process when using cooling towers and evaporative condensers for heat rejection. This is because they operate normally with circulating water at 32–42 °C which is the ideal growth range of Legionella. Dedicated water disinfection and prevention of stagnant water are required to comply with the local code of practice for prevention of Legionnaires' disease [34]. With regard to mist systems, the threat of spreading Legionella can be minimized by maintaining the water at below 25 °C under which Legionella is dormant. Furthermore, the amount and size of mists should be precisely controlled to facilitate full evaporation by the warm ambient air. To enhance water disinfection, each mist system can be provided with a UV lamp and its power rating is in a range of 40–120 W which accounts for only 0.6–1.8% of the total pump power.

4. Simulation of an office building and its chiller system

EnergyPlus [22] is a popular building energy simulation program [35] and was used to model a reference office building and its chiller system. It contains many innovative simulation features like user-configurable modular systems and building components that are integrated with a heat and mass balance-based zone simulation. This enhances the integrity of simulation results. With various

Table 2
General information on the reference office building.

General	
Gross floor area (GFA) (m^2)	51,840
Total air-conditioned area (m^2)	42,840 (82.6% GFA)
Floor dimension ($L \times W$) (m)	36 × 36
Area per floor (m^2)	1296
Air-conditioned area per floor (m^2)	1071
Floor to floor height (m)	3.2
External walls orientation	N/E/S/W
Construction details	
Window to wall ratio	0.5
U-value of wall (W/m^2 °C)	2.3
U-value of window (W/m^2 °C)	5.5
U-value of roof (W/m^2 °C)	0.7
Shading coefficient of glass	0.45
Zone design criteria	
Temperature (°C)	24
Relative humidity (%)	50
Ventilation rate (L/s/person)	10
Occupancy (m^2/person)	9
Equipment power density (W/m^2)	25
Lighting power density (W/m^2)	20
Air-conditioning system operating hours	
Weekdays	08:00–19:00
Saturdays	08:00–13:00
Sundays	Closed

system templates and the "autosize" feature, energy analysis on various system design options can be carried out expeditiously. Table 2 summarizes the general information on the building. The arrangement of the building is adopted to study the average energy performance of local office buildings [15]. It is a 40-floor building and each floor contains one internal thermal zone and four perimeter thermal zones facing North, East, South and West. The design criteria and operating schedules of various functional areas follow the specifications given in a local performance-based building energy code [36].

Table 3 shows basic information on the chiller and airside systems in the building. The chiller system contains four identical air-cooled centrifugal chillers designed to meet the peak cooling demand of 6044 kW calculated based on the cooling design dry bulb temperature and its coincident wet bulb temperature from the TMY. Chiller sequencing is implemented under which no additional chiller in the system starts to operate until each of the operating chillers is running at full load when meeting the changing building cooling loads. Each operating chiller runs at identical loads. The chilled water distribution circuit is designed with a primary loop having constant speed pumps coupled to the chillers and a secondary loop having variable speed pumps. A variable air volume (VAV) airside system is provided for all areas requiring air-conditioning. The systems were constructed by selecting proper system templates completed with the "autosize" feature and some default and built-in data. The sizing factor of one was specified in

Table 3
General information on the air-conditioning system.

Chiller system	
Chiller type	Air-cooled centrifugal
Number of chiller and pump sets	4
Nominal COP at full load	2.7
Design chilled water supply/return temperature (°C)	7/12.5
Design chilled water flow rate (m^3/s)	0.22
Chilled water loop	Constant primary-variable secondary
Airside system	
Type	Variable air volume (VAV)
Minimum airflow fraction	0.2
Fan motor efficiency	0.9

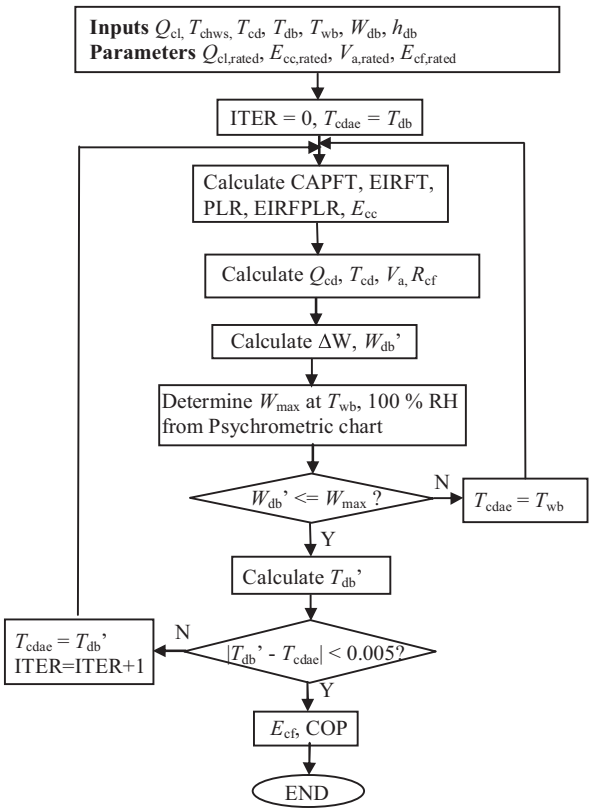

Fig. 6. Procedure for evaluating operating variables of the chiller with mist pre-cooling.

determining the capacity of system components. EnergyPlus computed the design capacity of each component and then performed hour-by-hour simulation of operating variables and electricity consumption. Simulation cases for different climate change scenarios were done by loading the respective weather files generated by CCWorldWeatherGen into EnergyPlus.

A standard template for chillers with default performance characteristics is available to model the performance of air-cooled centrifugal chillers under head pressure control. Yet there is no standard template capable of simulating air-cooled chillers with optimum condenser fan speed control (OCFSC). This analysis drew on the experimentally verified model given in [15]. Table 4 summarizes a list of equations inside the model to simulate the operating variables of the chillers with mist pre-cooling of air-cooled condensers. The model parameters were calibrated to represent the chillers with a nominal capacity of 1511 kW. Fig. 6 gives a flowchart showing how the operating variables were evaluated. To model the chiller performance with mist pre-cooling and OCFSC, the condensing temperature T_{cd} was no longer at a fixed set point of 45 °C. For a given combination of chiller loads and weather conditions, the rotating speed of the condenser fans was searched from a range of 5–100% of full speed that minimized the sum of compressor power, condenser fan power and mist pump power. Based on the optimal fan speed, the condensing temperature hovered closely above the dry bulb temperature within its operating boundaries.

5. Results and discussion

5.1. Monthly total system load under climate change scenarios

Fig. 7 shows the monthly total system load profiles in 2020, 2050 and 2080 in relation to the baseline (TMY). The monthly total system load will vary with the monthly mean dry bulb

Table 4
Modeling equations and parameters for air-cooled centrifugal chillers with advanced control.

Equations

$\mathrm{CAPFT} = a_0 + a_1(1.8T_{\mathrm{chws}} + 32) + a_2(1.8T_{\mathrm{chws}} + 32)^2 + a_3(1.8T_{\mathrm{cdae}} + 32) + a_4(1.8T_{\mathrm{cdae}} + 32)^2 + a_5(1.8T_{\mathrm{chws}} + 32)(1.8T_{\mathrm{cdae}} + 32)$
$a_0 = -0.09464899$; $a_1 = 0.0383407$; $a_2 = -0.00009205$; $a_3 = 0.00378007$; $a_4 = -0.00001375$; $a_5 = -0.00015464$

$\mathrm{EIRFT} = b_0 + b_1(1.8T_{\mathrm{chws}} + 32) + b_2(1.8T_{\mathrm{chws}} + 32)^2 + b_3(1.8T_{\mathrm{cdae}} + 32) + b_4(1.8T_{\mathrm{cdae}} + 32)^2 + b_5(1.8T_{\mathrm{chws}} + 32)(1.8T_{\mathrm{cdae}} + 32)$
$b_0 = 0.13545636$; $b_1 = 0.02292946$; $b_2 = -0.00016107$; $b_3 = -0.00235396$; $b_4 = 0.00012991$; $b_5 = -0.00018685$

$\mathrm{PLR} = Q_{\mathrm{cl}}/(Q_{\mathrm{cl,rated}}\ \mathrm{CAPFT})$

$\mathrm{EIRFPLR} = c_0 + c_1\mathrm{PLR} + c_2\mathrm{PLR}^2 + c_3T_{\mathrm{cd}} + c_4T_{\mathrm{cd}}{}^2 + c_5\mathrm{PLR}\,T_{\mathrm{cd}}$
$c_0 = 0.90961903$; $c_1 = 0.4989617$; $c_2 = 0.27488842$; $c_3 = -0.05064711$; $c_4 = 0.00086166$; $c_5 = -0.00554122$

$E_{\mathrm{cc}} = E_{\mathrm{cc,rated}} \times \mathrm{CAPFT} \times \mathrm{EIRFT} \times \mathrm{EIRFPLR}$ (kW)
$Q_{\mathrm{cd}} = Q_{\mathrm{cl}} + E_{\mathrm{cc}}$ (kW)
$V_{\mathrm{a}} = Q_{\mathrm{cd}}/(\rho_{\mathrm{a}}\,C_{\mathrm{pa}}\mathit{Eff}_{\mathrm{cd}}(T_{\mathrm{cd}} - T_{\mathrm{cdae}}))$ (m^3/s)
$R_{\mathrm{cf}} = 100\,V_{\mathrm{a}}/V_{\mathrm{a,rated}}$ (%)
$\mathit{Eff}_{\mathrm{cd}} = (T_{\mathrm{cdal}} - T_{\mathrm{cdae}})/(T_{\mathrm{cd}} - T_{\mathrm{cdae}})$
$E_{\mathrm{cf}} = E_{\mathrm{cf,rated}}R_{\mathrm{cf}}/100$ (kW)
$W_{\mathrm{db}}{}' = W_{\mathrm{db}} + m_{\mathrm{mist}}/(V_{\mathrm{a}}\rho_{\mathrm{a}})$ (kg/kg of dry air)
$T_{\mathrm{db}}{}' = (h_{\mathrm{db}} - 2501\,W_{\mathrm{db}}{}')/(1.006 + 1.805\,W_{\mathrm{db}}{}')$ (°C)

Parameters

$Q_{\mathrm{cl,rated}} = 1151$ kW; $E_{\mathrm{cc,rated}} = 560$ kW; $V_{\mathrm{a,rated}} = 140\ \mathrm{m}^3/\mathrm{s}$; $E_{\mathrm{cf,rated}} = 36$ kW

outdoor temperature with the highest value in July and the lowest value in January or February. The annual total system loads are 9,538,200 kWh in the TMY, 10,494,165 kWh in 2020, 11,464,932 kWh in 2050 and 12,884,487 kWh in 2080. This indicates that the annual system load increases by 10.0–14.9% over a period of 30 years. The annual electricity consumption of the chiller system will increase by 5.0–7.5% over an operating span of 15 years without a major retrofit if the system COP remains unchanged under the climate change scenarios.

5.2. Electricity consumption of the chiller system under climate change scenarios

Using EnergyPlus with a sophisticated chiller model, the electricity consumption of the chiller system serving the reference office building was evaluated on an hourly basis under the four operating schemes: HPC; HPC with mist pre-cooling; OCFSC; OCFSC with mist pre-cooling. Fig. 8 illustrates how the monthly total electricity consumption of chillers varied with different operating schemes in the TMY (baseline). Mist pre-cooling to air-cooled condensers performed very well with HPC or OCFSC in summer months, resulting in an apparent drop in the monthly total chiller electricity consumption. However, when mist pre-cooling was considered for chillers operating under HPC, a slight increase in the electricity consumption was observed in winter months due to a situation where the additional mist pump power outweighed the decrease of compressor power associated with a minor drop in the temperature of air entering the condenser.

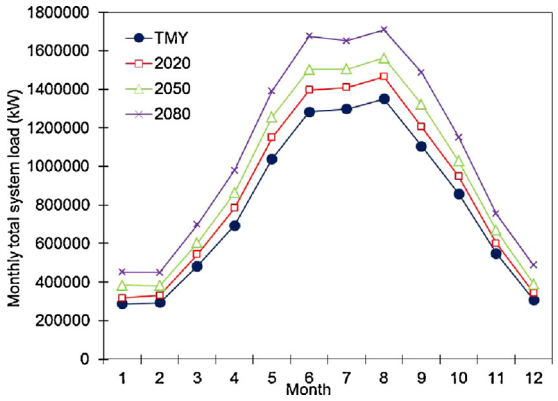

Fig. 7. Variation of monthly total system load in the TMY, 2020, 2050 and 2080.

Fig. 9 shows how the monthly total chiller electricity consumption under the climate change scenarios increases from the baseline (TMY). Regardless of the operating schemes, the higher increase in the electricity consumption occurs in winter months and this tends to correlate with the increase in the dry bulb temperature shown in Fig. 2. Different operating schemes lead to slightly different impacts on the chiller electricity consumption under the climate change scenarios. The use of mist pre-cooling to air-cooled condensers would temper the increasing chiller electricity consumption under the three climate change scenarios, when comparing Fig. 9(b) with (a) and (d) with (c). Indeed, Tables 5–8 show that from the TMY to 2080, a 16.96–18.58% decrease can be achieved in the annual electricity consumption of the system when applying OCFSC and mist pre-cooling. The average COP—the annual total system load in kWh divided by the total chiller electricity consumption in kWh—had a slight improvement in the operating schemes with mist pre-cooling. Without mist pre-cooling, the average COP tended to drop under the warmer climate, even when OCFSC was applied. Furthermore, the potential benefit of mist pre-cooling could be magnified under OCFSC, as reflected from Tables 5–8 that the percentage electricity savings from OCFSC + mist always exceed the sum of percentage electricity savings from OCFSC and HPC + mist. All these confirm that mist pre-cooling is a sustainable feature for air-cooled chillers in response to climate change.

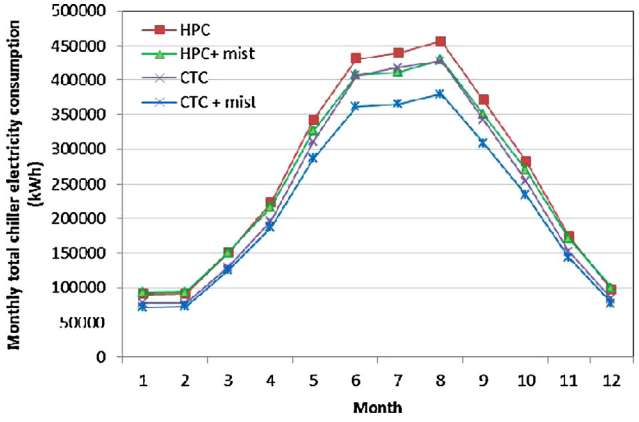

Fig. 8. Monthly total chiller electricity consumption with different operating schemes in the TMY.

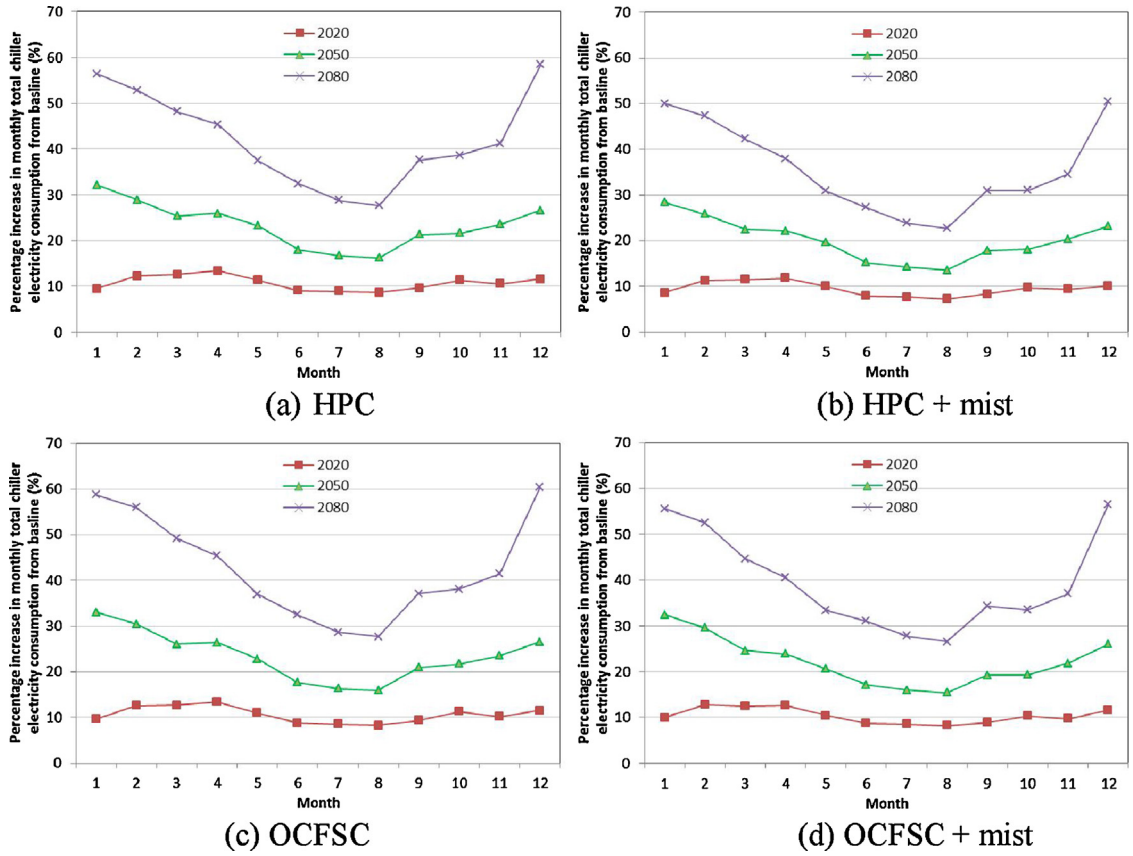

Fig. 9. Percentage increase in monthly total chiller electricity consumption in 2020, 2050 and 2080 from baseline under different operating schemes.

Table 5
Annual electricity consumption of chiller system in the TMY.

Operating scheme	HPC (baseline)	HPC + mist	OCFSC	OCFSC + mist
Pump consumption (kWh)	477,619	477,619	477,619	477,619
Chiller consumption (kWh)	3,147,486	3,020,814	2,876,675	2,613,631
Total system consumption (kWh)	3,625,105	3,498,434	3,354,294	3,091,250
Actual saving from baseline (kWh)	–	126,672	270,811	533,855
Percentage saving from baseline chiller consumption (%)	–	4.02	8.60	16.96
Average COP	3.03	3.16	3.32	3.65

Table 6
Annual electricity consumption of chiller system in 2020.

Operating scheme	HPC (baseline)	HPC + mist	OCFSC	OCFSC + mist
Pump consumption (kWh)	512,564	512,564	512,564	512,564
Chiller consumption (kWh)	3,468,822	3,290,619	3,164,285	2,867,417
Total system consumption (kWh)	3,981,386	3,803,183	3,676,849	3,379,981
Actual saving from baseline (kWh)	–	178,203	304,537	601,405
Percentage saving from baseline chiller consumption (%)	–	5.14	8.78	17.34
Average COP	3.03	3.19	3.32	3.66

Table 7
Annual electricity consumption of chiller system in 2050.

Operating scheme	HPC (baseline)	HPC + mist	OCFSC	OCFSC + mist
Pump consumption (kWh)	558,665	558,665	558,665	558,665
Chiller consumption (kWh)	3,808,972	3,565,318	3,475,912	3,127,831
Total system consumption (kWh)	4,367,637	4,123,983	4,034,577	3,686,496
Actual saving from baseline (kWh)	–	243,654	333,060	681,141
Percentage saving from baseline chiller consumption (%)	–	6.40	8.74	17.88
Average COP	3.01	3.22	3.30	3.67

Table 8
Annual electricity consumption of chiller system in 2080.

Operating scheme	HPC (baseline)	HPC + mist	OCFSC	OCFSC + mist
Pump consumption (kWh)	613,776	613,776	613,776	613,776
Chiller consumption (kWh)	4,316,804	3,967,698	3,941,826	3,514,755
Total system consumption (kWh)	4,930,580	4,581,474	4,555,602	4,128,531
Actual saving from baseline (kWh)	–	349,106	374,979	802,050
Percentage saving from baseline chiller consumption (%)	–	8.09	8.69	18.58
Average COP	2.98	3.25	3.27	3.67

Table 9
Results of correlation analysis on mist generation rate with climatic and operating variables.

Variable	T_{db}	RH	T_{wb}	W_{db}	h_{db}	PLR	V_a
HPC + mist							
Pearson correlation	−0.052	−0.911	−0.139	−0.230	−0.118	0.232	0.412
p-Value	0.004	0.000	0.000	0.000	0.000	0.000	0.000
OCFSC + mist							
Pearson correlation	0.442	−0.274	0.437	0.353	0.422	0.561	0.538
p-Value	0.000	0.000	0.000	0.000	0.000	0.000	0.000

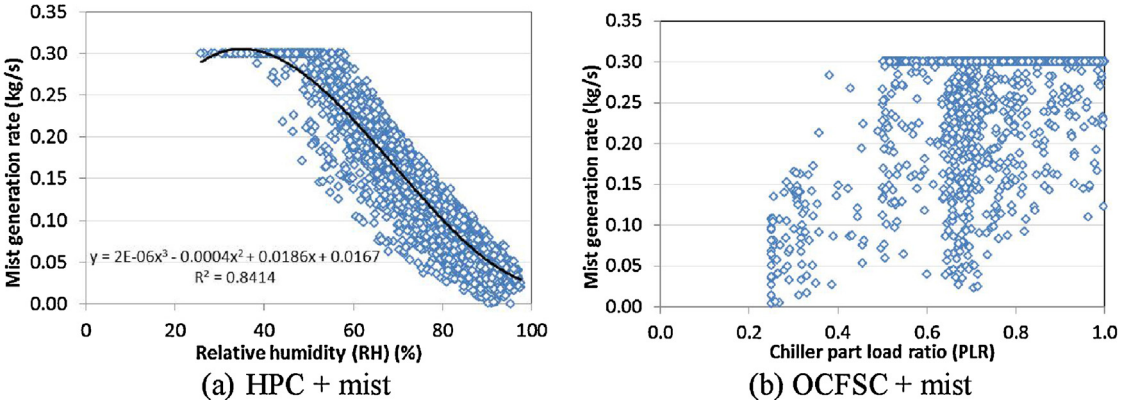

Fig. 10. Plots of mist generation rate against the variables with the highest Pearson correlation.

5.3. Control of mist generation rate

Having identified the benefit of applying mist pre-cooling to air-cooled condensers, it is important to understand how to control the mist generation rate under various operating conditions. A bivariate correlation analysis [37] was conducted between the required mist generation rate m_{mist} and a set of climatic and operating variables: T_{db}, RH, T_{wb}, W_{db}, h_{db}, PLR and V_a. This analysis helps ascertain if the required m_{mist} can be determined by any one of the variables. Table 9 summarizes the Pearson correlation coefficients and *p*-values of their correlation under the operating schemes: HPC + mist and OCFSC + mist. The correlation of m_{mist} with all the variables is considered significant because all the *p*-values are below 0.005—a significant level of 0.01 (2-tailed).

Fig. 10 shows scatter plots of m_{mist} against the variables with the highest Pearson correlation. When the chiller operated under HPC, it is possible to adjust the mist generation rate based on relative humidity to obtain near optimal mist control. Indeed, if the regression curve in Fig. 10(a) is used to determine the required mist generation rate, the mist system will operate more frequently, enabling the annual chiller electricity consumption to drop by 3.98% which is only 0.04% less than the saving of 4.02% in the case of HPC + mist with the TMY shown in Table 5. Yet for the chiller operating under OCFSC, the adjustment of mist generation rate is more complicated as the mist generation rate tends to spread out when plotting against each of the variables. An example of scattering between the mist generation rate and chiller part load ratio is provided in Fig. 10(b). It is not feasible to achieve optimal mist control based on a single variable like the chiller part load ratio. Furthermore, it may not be feasible to use a combination of measured variables to evaluate the required mist generation rate and implement the feed-forward control. Alternatively, it is possible to apply the feed-back control to regulate the mist generation rate based on the temperature of pre-cooled air entering the condenser. The mist generation rate can be increased until the air temperature monitored after precooling reaches the lowest level—the coincident wet bulb temperature. Indeed, the mist system control, the condenser fan control and the compressor control interact with each other. All these call for development of an advanced optimization control strategy so as to determine the number of mist generation pumps required to minimize the sum of the compressor power, condenser fan power and mist pump power in all operating conditions. It is important to measure the rate of change of the individual power of the compressor, condenser fans and mist generation pump to examine the optimal number and speed at which the aggregate power is minimized. The effectiveness of the mist system under different heat rejection airflow rates remains to be investigated and this constitutes the future experimental work by the authors.

6. Conclusions

This paper demonstrates how mist pre-cooling to air-cooled condensers helps enhance the sustainability of air-cooled chiller systems under climate change. Weather data of three climate change scenarios in 2020, 2050 and 2080 were generated by

CCWorldWeatherGen. In simulating the cooling demand and hourly electricity consumption of an air-cooled chiller system serving a reference office building, EnergyPlus was used together with an experimentally verified chiller model capable of analysing advanced control strategies. It is found that mist pre-cooling of air-cooled condensers can complement optimal condenser fan speed control to boost the chiller COP under the warmer future climate, resulting in an electricity savings of 16.96–18.58% in the TMY and 2080. When the chillers operate under HPC, the control of mist generation rate is straightforward and done by operating the mist pump based on relative humidity which can be measured directly. To implement optimal condenser fan speed control with mist pre-cooling, more sophisticated feed-back control is required to regulate the mist generation rate in order to maximize the overall chiller COP. It remains to be carried out experimental tests of an air-cooled chiller equipped with a mist system to identify the dynamic characteristics of cooling effectiveness when operating under the optimal condenser fan speed control. The experimental findings will help fine-tune the control algorithm of a mist system and hence to verify the improvement of an actual chiller COP under the optimal control.

The significance of this study is to promote mist pre-cooling as a sustainable feature for air-cooled chillers under climate change, considering that their application is still unavoidable where water conservation is concerned. Given the potential benefits of the mist application, chiller designers and manufacturers should devote further development on design and installation guidelines on mist systems used for air-cooled chillers. It remains to be formulated an assessment method to quantify the effectiveness of mist pre-cooling for chillers operating under various climatic zones.

Acknowledgements

The work described in this paper was supported by a grant from the Research Grant Council of the Hong Kong Special Administrate Region, Project A/C Code: G-YK51 and a grant from the College of Professional and Continuing Education, an affiliate of The Hong Kong Polytechnic University, Project A/C 4.8C.xx.EZ20.

References

[1] J. Jahanbani Ardakani, F. Fattahi Ardakani, S.H. Hosseinian, A novel approach for optimal chiller loading using particle swarm optimization, Energy and Buildings 40 (2008) 2177–2187.
[2] F.W.H. Yik, J. Burnett, I. Prescott, Predicting air-conditioning energy consumption of a group of buildings using different heat rejection methods, Energy and Buildings 33 (2001) 151–166.
[3] R.K.L. Chan, E.W.M. Lee, R.K.K. Yuen, An integrated model for the design of air-cooled chiller plants for commercial buildings, Building and Environment 46 (2011) 196–209.
[4] Y.C. Chang, Optimal chiller loading by evolution strategy for saving energy, Energy and Buildings 39 (2007) 437–444.
[5] W.S. Lee, Y.T. Chen, Y.C. Kao, Optimal chiller loading by differential evolution algorithm for reducing energy consumption, Energy and Buildings 43 (2011) 599–604.
[6] Y.J. Sun, S.W. Wang, G.S. Huang, Chiller sequencing control with enhanced robustness for energy efficient operation, Energy and Buildings 41 (2009) 1246–1255.
[7] Y.H. Song, Y. Aksashi, J.J. Yee, Energy performance of a cooling plant system using the inverter chiller for industrial building, Energy and Buildings 39 (2007) 289–297.
[8] R. Saidur, M. Hasanuzzaman, T.M.I. Mahlia, N.A. Rahim, H.A. Mohammed, Chillers energy consumption, energy savings and emission analysis in an institutional buildings, Energy 36 (2011) 5233–5238.
[9] K.A. Manske, D.T. Rendl, S.A. Klein, Evaporative condenser control in industrial refrigeration systems, International Journal of Refrigeration 34 (2001) 676–691.
[10] K.T. Chan, F.W. Yu, Applying condensing-temperature control in air-cooled reciprocating water chillers for energy efficiency, Applied Energy 72 (2002) 565–581.
[11] A.A. Chowdhury, M.G. Rasul, M.M.K. Khan, Modelling and analysis of air-cooled reciprocating chiller and demand energy savings using passive cooling, Applied Thermal Engineering 29 (2009) 1825–1830.
[12] H. Zhang, S.J. You, H.X. Yang, J.L. Niu, Enhanced performance of air-cooled chillers using evaporative cooling, Building Services Engineering Research and Technology 21 (4) (2000) 213–217.
[13] E. Hajidavalloo, H. Eghtedari, Performance improvement of air-cooled refrigeration system by using evaporatively cooled air condenser, International Journal of Refrigeration 33 (2010) 982–988.
[14] J. Yang, K.T. Chan, X.S. Wu, F.W. Yu, X.F. Yang, An analysis on the energy efficiency of air-cooled chillers with water mist system, Energy and Buildings 55 (2012) 273–284.
[15] F.W. Yu, K.T. Chan, Improved energy performance of air-cooled chiller system with mist pre-cooling, Applied Thermal Engineering 31 (2011) 537–544.
[16] Air-Conditioning Heating and Refrigeration Institute. AHRI Standard 551/591: Performance Rating of Water Chilling and Heat Pump Water-Heating Packages using the Vapor Compression Cycle, Author Press, Arlington, VA, 2011.
[17] J.C. Lam, K.K.W. Wan, K.L. Cheung, An analysis of climatic influences on chiller plant electricity consumption, Applied Energy 86 (2009) 940–993.
[18] J. Yang, K.T. Chan, X.S. Wu, X.F. Yang, H.Y. Zhang, Performance enhancement of air-cooled chillers with water mist: experimental and analytical investigation, Applied Thermal Engineering 40 (2012) 114–120.
[19] F.W. Yu, K.T. Chan, Simulation and electricity savings estimation of air-cooled centrifugal chiller system with mist pre-cooling, Applied Energy 87 (2010) 1198–1206.
[20] F.W. Yu, K.T. Chan, Modelling of improved energy performance of air-cooled chillers with mist pre-cooling, International Journal of Thermal Sciences 48 (2009) 825–836.
[21] A.L.S. Chan, T.T. Chow, K.F. Fong, Z. Lin, Generation of a typical meteorological year for Hong Kong, Energy Conversion and Management 83 (1) (2006) 87–96.
[22] EnergyPlus energy simulation software, available at: http://apps1.eere.energy.gov/buildings/energyplus/energyplus_about.cfm
[23] L. Guan, Preparation of future weather data to study the impact of climate change on buildings, Building and Environment 44 (2009) 793–800.
[24] Climate Change World Weather File Generator for World-Wide Weather Data – CCWorldWeatherGen, available at: http://www.serg.soton.ac.uk/ccworldweathergen/
[25] Intergovernmental Panel on Climate Change (IPCC), homepage, available at: http://www.ipcc.ch/
[26] M.F. Jentsch, A.S. Bahaj, P.A.B. James, Climate change future proofing of buildings – generation and assessment of building simulation weather files, Energy and Buildings 40 (2008) 2148–2168.
[27] D.H.W. Li, L. Yang, J.C. Lam, Impact of climate change on energy use in the built environment in different climate zones – a review, Energy 42 (2012) 103–112.
[28] K. Lee, G.J. Levermore, Weather data for future climate change for South Korean building design: analysis for trends, Architectural Science Review 53 (2010) 157–171.
[29] TMY weather file for Hong Kong, available at: http://apps1.eere.energy.gov/buildings/energyplus/cfm/weather_data3.cfm/region=2_asia_wmo_region_2/country=CHN/cname=China
[30] CCWorldWeatherGen user manual, available at: http://www.serg.soton.ac.uk/ccworldweathergen/manual_weather_tool.pdf
[31] A. Sturman, N. Tapper, The Weather and Climate of Australia and New Zealand, 2nd ed., Oxford University Press, Melbourne, 2005.
[32] R. Aguiar, M. Oliveira, H. Gonccedilalves, Climate change impacts on the thermal performance of Portuguese buildings. Results of the SIAM study, Building Services Engineering Research and Technology 23 (2002) 223–231.
[33] S.E. Belcher, J.N. Hacker, D.S. Powell, Constructing design weather data for future climates, Building Services Engineering Research and Technology 26 (1) (2005) 49–61.
[34] Prevention of Legionnaires' Disease Committee, Hong Kong, Prevention of Legionnaires' disease – code of practice, 2012 edition, available at: http://www.emsd.gov.hk/emsd/e_download/pps/others/COP-PLD_2012.pdf
[35] D.B. Crawley, L.K. Lawrie, F.C. Winkelmann, W.F. Buhl, Y.J. Huang, C.O. Pedersen, R.K. Strand, R.J. Liesen, D.E. Fisher, M.J. Witte, J. Glazer, EnergyPlus: creating a new-generation building energy simulation program, Energy and Buildings 33 (2001) 319–331.
[36] Electrical and Mechanical Services Department, Performance-based building energy code, available at: http://www.emsd.gov.hk/emsd/eng/pee/eersb.shtml
[37] R.L. Sims, Bivariate Data Analysis: A Practical Guide, Nova Science Publishers, Inc., Huntington, NY, 2000.